Boise State University
ScholarWorks

Civil Engineering Faculty Publications and Presentations

Department of Civil Engineering

Electromagnetically Induced Transport in Water for Geoenvironmental Applications

Arvin Farid
Boise State University

Atena Najafi
Boise State University

Mahsa Azad
Boise State University

Jim Browning
Boise State University

Elisa Barney Smith
Boise State University

Electromagnetically Induced Transport in Water for Geoenvironmental Applications

Arvin Farid
Associate Professor
Department of Civil and Environmental Engineering
Boise State University

Jim Browning
Associate Professor
Department of Electrical and Computational Engineering
Boise State University

Atena Najafi
Graduate Research Assistant
Department of Civil and Environmental Engineering
Boise State University

Elisa Barney Smith
Associate Professor
Department of Electrical and Computational Engineering
Boise State University

Mahsa Azad[3]
Graduate Research Assistant
Department of Civil and Environmental Engineering
Boise State University

Abstract

Air sparging is a popular soil remediation technique that enables the removal of contaminants through diffusing air into soil. The removal process is, however, slow. The goal of this work is to study the effect of electromagnetic (EM) waves —with minimal heat generation— on transport mechanisms such as diffusion, in order to improve airflow or contaminant transport in order to expedite the cleanup process using air sparging or similar technologies. This effect is studied through an experimental setup that examines the diffusion of a nonreactive dye in water under EM waves at a range of frequencies (50-200 MHz). The electric field was simulated using COMSOL Multiphysics for better three-dimensional (3D) visualization and analysis and then validated using the experimental measurements. A dielectrophoretic study was then performed using the simulated electric field. Various dye flows under EM stimulation at different frequencies were compared. At 65 MHz and 76 MHz, the dye flow was in the direction of the dielectrophoretic forces, which are believed to be the governing mechanism for the EM-stimulated dye transport.

Keywords: Air Sparging, Electromagnetic, Resonant Cavity, Dielectrophoresis.

1. Introduction

Remediation of contaminated soil and groundwater has become an important area of interest to federal and state agencies in recent decades. Several remediation techniques have been used for removal of the contaminants among which, air sparging (Johnson et al., 1998) is very popular. In-situ air sparging (AS), is a technique in which air or oxygen is injected into water-saturated zones in order to remove organic contaminants by a combination of volatilization and aerobic biodegradation processes. This technology involves the injection of contaminant-free air into water-saturated zones of the subsurface to enable the phase transfer of organic contaminants from a dissolved or adsorbed state to a vapor phase. Air sparging is most often used with soil vapor extraction (SVE), which creates a negative pressure in the unsaturated zone —above the water-table level— through a series of extraction wells to control the vapor plume migration and to capture vapors. Despite the impressive results, the effectiveness of air sparging is limited because it is considered a semi-random remediation process (Braida and Ong, 2001). Air can flow more easily in partially saturated media compared to water-saturated ones. Therefore, because of the limited number of formed air channels, several portions of contaminated regions would not be exposed to the air and would remain untreated.

Several methods have been proposed to improve AS, including pulsation of injection pumps at different periods and patterns (Benner et al., 2002), which is very time consuming. The use of direct electric current, DC, or alternating current, AC (Suthersan and Raton, 1999), can enhance air sparging but create uncontrolled heat, and DC alters the pH of soils, adversely affecting microbial life in soils. Electromagnetic (EM) heating of the soil (Vermeulen and McGee, 2000) was also attempted to improve air sparging or other remediation technologies. The main objective of this work is to study the effect of electromagnetic waves on transport mechanisms in saturated media at frequencies where heat generation is minimal. An advantage of EM over other enhancement methods such as DC is that EM waves can be applied at low MHz frequencies (e.g., 10-500 MHz) and lower EM power, hence, generating a small amount of heat in the medium and not altering the PH of the environment.

The transport of a nonreactive inert dye in water was studied as a visible analogy to the airflow occurring in AS in saturated media. The goal of this study was to find the governing phenomenon that directs the dye flow under EM stimulation. Dielectrophoresis was specifically investigated as a potential governing mechanism behind this effect. Studying the correlation between the magnitude, frequency, and radiation pattern of EM waves and the transport rate was another objective of this work.

2. Background

One of the mechanisms potentially governing the transport of the dye through the water medium, at all times, is diffusion. The theory of diffusion describes the spread of particles through random motion that on average moves more dye from regions of higher concentration to regions of lower concentration. Fick's second law (Cussler, 1997) describes the diffusion of the dye.

$$\frac{\partial C}{\partial t} = -\vec{\nabla} \cdot \vec{F} = \frac{\partial}{\partial x}\left(D_x \frac{\partial C}{\partial x}\right) + \frac{\partial}{\partial y}\left(D_y \frac{\partial C}{\partial y}\right) + \frac{\partial}{\partial z}\left(D_z \frac{\partial C}{\partial z}\right) \tag{1}$$

where t is time (s). For a homogenous and isotropic medium such as the water medium of our experiment, ($D_x = D_y = D_z = D$).

Dielectrophoresis is a possible mechanism behind dye motion under EM stimulation (Azad et al., 2012). An alternating electric field induces a polarization in particles in the medium, and the particles are subject to a net force from the electric-field gradient regardless of the particles' charge. The result of this force, $\vec{F}_{DEP}$ (N), is described by the following (Jones, 2003) equation.

$$\vec{F}_{DEP} = 2\pi r^3 \varepsilon_m^* \, \text{Re}\left\{\frac{\varepsilon_p^* - \varepsilon_m^*}{\varepsilon_m^*}\right\} \nabla |\vec{E}|^2 \tag{2}$$

where $\vec{E}$ is the nonuniform electric field (V/m), and r is the radius (m) of the homogeneous sphere representing particles with no net charge. When the dielectric permittivity of particles is higher than that of the background medium, the particles will move toward the area of lower electric-field intensity and vice versa.

A resonant cavity, an important component of the present setup, is a waveguide with enclosed front and back faces. Loop coupling is a loop antenna oriented in such a way that the plane of the loop is perpendicular to the magnetic field lines where the magnetic field is at its maximum. For the cavity used here, the inductive excitation (e.g., using loop coupling) is practically a better choice than the capacitive method (e.g., using dipole antennae), since more energy can be coupled into the cavity.

3. Materials and Methods

3.1 Experimental Setup

The experimental setup consists of a 40-cm × 40-cm × 40-cm acrylic box containing deionized, deaerated water with a 38-cm × 38-cm × 38-cm RF (radio-frequency) resonant cavity inside it (Figure 1).
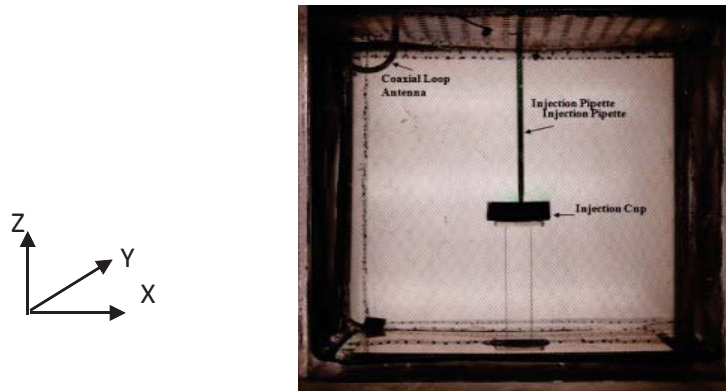

FIG. 1. Medium under test for the setup showing the acrylic box, resonant cavity filled with water, injection cup, injection pipette, and loop antenna.

The cavity structure was built using copper mesh screens instead of solid copper plates to enable imaging and visualization. It is noteworthy that the opening diameter of the copper mesh is ~3 mm (1/8 inch), which is much smaller than the wavelength of the applied 50-200 MHz frequency waves in water (≈160 mm -660 mm). A coaxial loop antenna made of an RG8 coaxial cable coupled to the resonant cavity and connected to the EM source was used to launch EM waves into the medium. The inner conductor passes through a brass piece welded to the top copper boundary, hence sharing the same electric ground as the outer conductor, to provide electrical continuity to the resonant cavity. A continuous wave (CW) radio-frequency signal was generated using an HP E4400B signal generator. A Model 100 LMB amplifier, manufactured by Amplifier Research, was used to amplify the generated signal. To maximize the amplifier output (i.e., forward power) to be input into the testing medium and minimize the reflection back to the amplifier, a matching network was used. The matching network included two two-gang variable capacitors placed within aluminum BUD box, used to match the impedance of the testing medium to the 50-Ω impedance of the amplifier.

An inert, nonreactive, water-based dye (green McCormmick food-coloring) was used as the diffusing matter to allow the visualization of the transport inside the medium. A clear acrylic table was built to allow the introduction of the dye close to the center of the medium (far from the cavity boundaries). A circular plastic cup with a radius of 30 mm was glued to the top plate of the injection table.

Digital imaging was used to analyze the transport of the dye. Images were captured using a Cannon Rebel T2i 18-MegaPixel digital camera at 30 second intervals. The pixel values of the two-dimensional (2D) digital images correlated to the dye concentration integrated along corresponding lines of sight almost parallel to the Y axis (i.e., perpendicular to the image).

The electric field was mapped in the region under test using a 50-Ω, RG-402, coaxial probe controlled by a three-dimensional (3D) translation table. The probe was connected to a spectrum analyzer and was moved to the nodes of any desired 3D grid. The monopole probe was vertically polarized and collected measurements dominated by the Z component of the electric field. However, a full 3D vector electric field was necessary to understand the correlation between the RF radiation pattern and the dye transport. Therefore, the electric field pattern was simulated at various frequencies using the COMSOL software, and its Z component was validated against the experimentally mapped electric field. Figure 2 shows typical measured and simulated contour maps on one depth (vertical) slice at 65 MHz. Slice 1 is 11 cm from the center of the box. The temperature of the water close to the antenna body was recorded at different EM stimulation frequencies in order to differentiate the effect of temperature on the dye flow from the effect of RF waves.
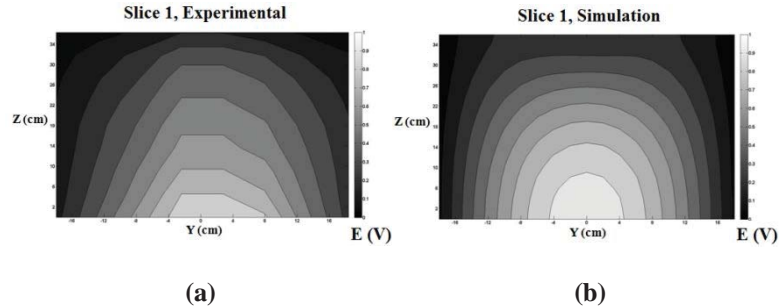
3

(a)   (b)

FIG. 2. Normalized electric field map (a) Slice 1, experimentally measured; (b) Slice 1.

3. Results and Discussions

3.1 Unstimulated Tests

After complete injection of the dye, small portions of the dye rose from the cup and then descended downward because the dye density was slightly larger than that of water (1 g/cm3). There was a relatively random time interval (5 to 12 minutes) at which the dye rose out of the cup. However, approximately 1 hour past the start of the experiment, this time interval decreased, and more continuous risings were observed. Figure 3a shows an example of the dye transport in an unstimulated test.

(a)   (b)   (c)   (d)
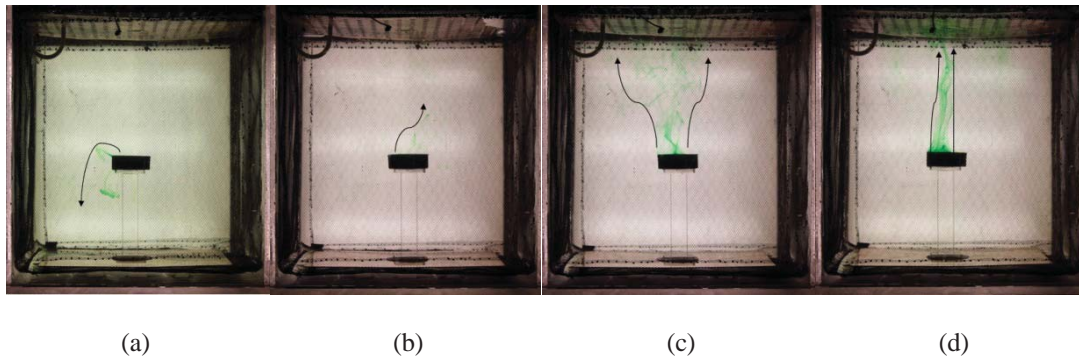
FIG. 3. Dye transport during (a) unstimulated test; dye randomly rises out of injection cup and descends; and dye flow in an EM-stimulated experiment at 65 MHz frequency after 20 minutes of stimulation and at the power level of: (b) 10 W, (c) 20 W, and (d) 30 W, dye rises out of injection cup toward top boundary.

3.2 Stimulated Tests

When the medium was stimulated at the frequency of 65 MHz, there was an upward flow of the dye. Portions of the dye rose out of the cup then moved toward the top boundary of the resonant cavity. After reaching the top boundary, the dye spread horizontally in random directions. The stimulated experiment was performed at 10, 20, and 30 W to investigate the effect of the EM power level. Increasing the EM power increased the upward dye flow. Figures 3b, 3c, and 3d illustrate the flow of the dye 20 minutes after the dye injection at power magnitudes of 10, 20, and 30 W, respectively. The threshold of power needed to electromagnetically induce the upward dye transport is $P = 10$ W at the frequency of $f = 65$MHz.

3.3 Radiation Pattern and Frequency Effects

Although only the 65 MHz simulation was successfully validated experimentally, the experiment was repeated for other frequencies as well. The choice of the frequency was based on the quality of the impedance-matching and achieved low reflection monitored by the spectrum analyzer. As a result, several tests were performed at 60, 69, 75, and 77 MHz at an RF power of 30W. Unlike the tests performed at 65MHz, during the stimulation at these other frequencies —except for 75MHz— the flow of the dye was observed to be similar to the unstimulated tests. In other words, the stimulation had

no apparent effect on the flow of the dye. At 75 MHz, the dye remained inside the cup as long as the medium was stimulated and the power was above 3 W. The simulated electric-field pattern seems to support this phenomenon according to a potential dielectrophoretic nature. However, the experimental electric-field measurements showed no consistency with the simulation.

3.4 Isolating Effect of Temperature on Dye Flow

The change of temperature over time for different frequencies at a distance of 1 cm from the center of the loop antenna –where the strongest temperature rise was expected due to resistive heat generation at the proximity to the heat source was monitored. The maximum change in temperature within the period of stimulation– was less than 1°C for all frequencies. The observed rise in the temperature was the same for all frequencies. This suggests that the flow of the dye is not dominated by a convective flow and is mostly due to other phenomena related to the electromagnetic field.

3.5 Electric-Field Pattern Effect

The validated simulated electric field, exported into MATLAB, contains the X, Y, and Z components of the electric field at nodes spaced on a 2-cm grid within the cavity. A script ("*m.file*") was developed using a forward finite difference method to calculate the gradient of the squared electric field ($\vec{\nabla} \mid E \mid^2$) based on Eq. 3.

$$\vec{\nabla} \mid E \mid^2 = \nabla_x \mid E \mid^2 \hat{i} + \nabla_y \mid E \mid^2 \hat{j} + \nabla_z \mid E \mid^2 \hat{k}$$

$$= \frac{\mid E \mid^2_{i+1,j,k} - \mid E \mid^2_{i,j,k}}{dx} \hat{i} + \frac{\mid E \mid^2_{i,j+1,k} - \mid E \mid^2_{i,j,k}}{dy} \hat{j} + \frac{\mid E \mid^2_{i,j,k} + 1 - \mid E \mid^2_{i,j,k}}{dz} \hat{k} \qquad (3)$$

Three matrices for the three components of the gradient of the squared electric field were computed. However, the dye concentration at each node within the images represents the concentration integrated over the line of sight (in the Y direction, i.e., perpendicular to the image). Hence, the X and Z components of the gradient of the squared electric field were integrated over the Y-axis. Figures 4a and 4b represent the contour maps of the Z and X components of the $\vec{\nabla} \mid E \mid^2$ vector.

According to Figure 4a, the Z-component of $\vec{\nabla} \mid E \mid^2$ is negative with an increasing magnitude toward the top. As a result, because of the smaller dielectric constant of the dye compared to that of water (≈ 81), the dielectrophoretic force on the dye is in the positive Z direction (i.e., upward) at 65 MHz. This is in agreement with the results from the experimental field investigation as well.
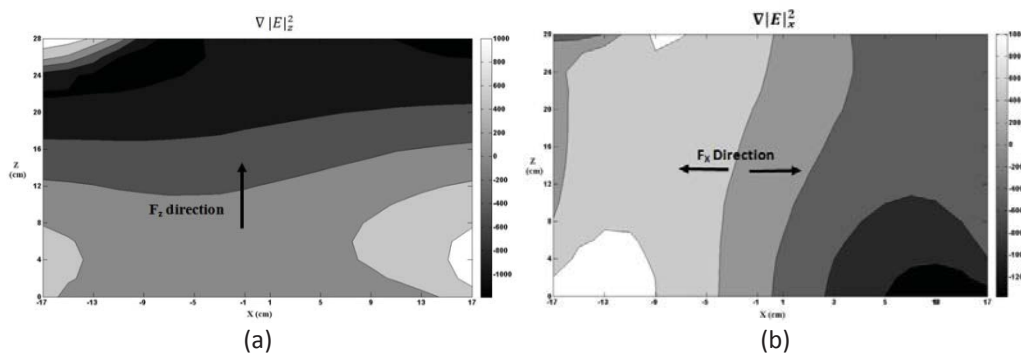

FIG. 4. Contour maps of the simulated $\vec{\nabla} \mid E \mid^2$ (V²/m³) according to COMSOL Multiphysics results at 65 MHz: (a) Z component, $\vec{\nabla}_z \mid E \mid^2$, and (b) X component, $\vec{\nabla}_x \mid E \mid^2$

On the other hand, $\vec{\nabla}_x |E|^2$ (i.e., the X-component of the $\vec{\nabla} |E|^2$ vector) creates a force that drags the dye toward the side walls of the cavity. The magnitude of the forces in the X direction is almost ½ of the magnitude of the vertical forces. As a result and in agreement with the experimental observation, the upward flow of the dye dominates the horizontal flow. The horizontal flow appears to dominate after the dye approaches near the top boundary where the upward flow has slowed or stopped. Since the dye has a flow moving both right and left after it reaches the top boundary, the observed horizontal flow can be interpreted as a mix of dielectrophoresis and diffusion.

3.6 Digital Analysis and Evaluation

Digital-image analysis was performed to extract quantifiable information from the images of dye transport in RAW format. RAW-format images were then converted into the TIFF format and imported into MATLAB in a matrix format. The averaged, background (i.e., box and water but no dye) image was subtracted from every other image, leaving only the transporting dye. The elements of the resulting matrices represent the intensity of pixels at different locations in the box as a representative of dye concentration. Following analyses were then performed.

Pixel Intensity Summation: a comparison of the summation of pixel intensities for the tests can be performed to evaluate the variations of the total amount of dye that leaves the injection cup upward into the upper zone. A zone shown in Figure 5a was selected to measure the amount of dye that had left the injection cup representing the main finger formed in each test. The summation was performed on the sets of experiments performed at 65 MHz (10 W, 20 W, and 30W) and at 75 MHz (30 W), as well as the unstimulated test. Figure 6 indicates the plot of the summation of pixel intensities over time for these tests.
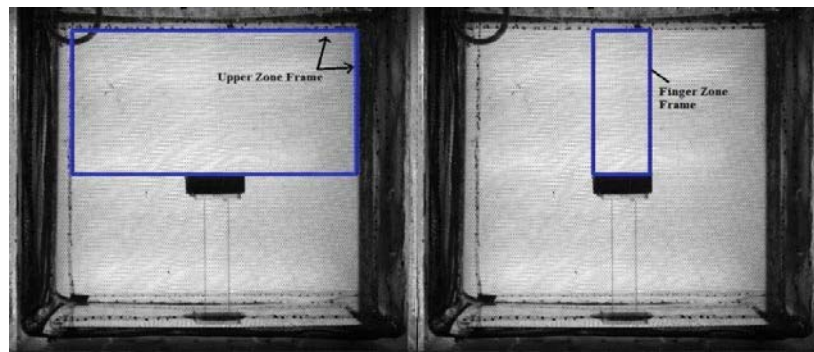

FIG. 5. (a) Study zone, referred to as upper zone, in "Intensity Summation Analysis" and (b) Study zone, referred to as finger zone, in the "Finger-Height Analysis."

Because no dye transport was observed for the tests performed at 75 MHz, it was, therefore, expected that the summation of pixel values for this test be constant (zero) over time. The plot shows some variations over time attributed to the errors associated with the background noise. In general, the average value did not increase or decrease. The similar range of concentration data associated with the unstimulated test and the stimulated test at 10W proves that the amount of the dye entering this zone was not large enough to overcome the error values. In summary, the change of the sum of pixel intensities over time for the unstimulated test, stimulated test at 75 MHz (even at 30 W of power), and 65 MHz (with a power less than 10W) followed the same pattern with the average unchanged.

The plot of pixel values over time for the stimulated tests at 65 MHz (at 20 W and 30 W), on the other hand, shows different results. The sum of adjusted pixel intensities increased over time for these two tests, meaning pixels became darker. This refers to the presence of more dye in the upper region.

In order to quantify the variations in the sum of pixel values over time for each test, the relative change (%) of the summation is also calculated. Therefore, the last three data sets (at t = 105 min, t = 106.5 min., and t = 108 min. after the beginning of the stimulation) were averaged and subtracted from the initial dataset (t= 0 min.) of the curves of Figure 6a. The relative change (%) was calculated and plotted versus power, shown in Figure 6b.

Several other finger-characteristic parameters were calculated to understand the shape of each finger. These characteristic parameters include finger height and width. A finger zone is defined in images (e.g., shown in Figure 3b). This zone includes the main dye finger for the majority of the time during the upward flow of the dye, when the medium is electromagnetically stimulated (at 65 MHz at 10, 20, and 30 W power). This study is limited to the test performed at 65 MHz because of stronger, more controlled finger movements at this specific frequency due to the size of the cavity. The number of pixels containing enough dye (above a consistent threshold representing visible fingers) was recorded versus elevation within the selected zone at different times. The number represents the width of the finger. This method enabled a study of the finger-width profile for each test over time. As seen in Figure 6c (for the test performed at 65 MHz at 10 W of power) the finger width was almost constant at all elevations and was always smaller than the one for 20 and 30 W power levels. For the 20 W cases, the finger width was almost constant at all elevations as well but was larger than that of the 10-W cases. This was representative of a more concentrated upward dye flow in the 20-W cases compared to the 10-W cases that were not focused and dispersed gradually. For the test at 30 W, the plot shows that the width decreased rapidly with increasing elevation above the injection cup. However, the fingers became darker (the intensity of these pixels increased drastically). The digital pictures associated with this test confirms much darker, still more focused, fingers moving faster and in a more straight, focused, and powerful shape at 30 W.

(a)   (b)   (c)
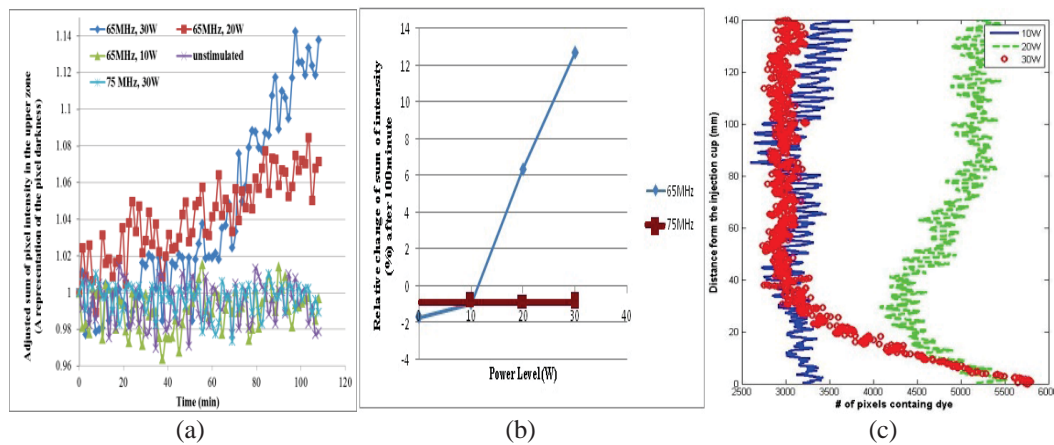
FIG. 6. Plot of adjusted sum of image-pixel intensities (representing transported dye amounts) for unstimulated test (summation performed over highlighted upper zone in digital images); three stimulated tests at 65 MHz at power levels of 10 W, 20 W, and 30 W; and one stimulated test at 75 MHz at 30 W of power versus: (a) time, (b) power, and (c) Plot of total number of pixels containing enough dye to be considered a finger accumulated over time versus elevation above injection cup.

Conclusion

The effect of EM waves on the flow of a nonreactive dye within a resonant cavity was studied in this paper. When the medium was not stimulated by the electromagnetic waves, the dye sporadically rose out of the injection cup and then randomly descended toward the bottom of the medium. When the medium was stimulated at the frequency of 65 MHz, the dye moved towards the top boundary of the medium. The flux of this upward dye transport increased as a function of the input EM power. The stimulation was also repeated for the frequencies of 60, 69, 75, and 77 MHz. The results show that except for the frequency of f = 75 MHz, the dye flows similar to the unstimulated test within the resonant cavity. At 75 MHz, however, the dye was contained inside the cup so long as the medium was stimulated.

The medium temperature was monitored during experiments and observed to be minimal. Similar temperature variations were observed for all frequencies. The study, therefore, proves that the small temperature increase within the medium and convective flow are not the reason –or at least not the dominating reason— behind the different dye flow patterns under EM stimulation.

At 65 MHz, the transport pattern was consistent with the dielectrophoretic force expected based on the simulated and experimentally measured electric-field patterns. The flux of the dye flow and the width of the dye fingers increase when the power is increased from 10 W to 20 W. On the other hand, when the power is raised to 30 W, the dye flux increases. However, the finger width becomes larger at the vicinity of the injection cup but then decreases at higher elevations. In

other words, the finger becomes more focused (i.e., narrower but darker). This can be due to the strong dielectrophoretic force compared to diffusion at 30 W compared to the 10-W and 20-W cases. This results in darker, more focused fingers at the 30-W case compared with weaker, wide-spread fingers at 10-W and 20-W cases.

Acknowledgement

References

Azad, M., Sangrey, H.D.O, Farid, A., Browning, J., and Barney-Smith, E. (2012). "Electromagnetic stimulation of two-phase transport in water-saturated media for geoenvironmental applications." *ASTM Geotechnical Testing Journal*, Vol.36, No. 1: 97-106

Balanis, C.A. (1989). *Advanced Engineering Electromagnetics*, first Edition, John Wiley & Sons, New York.

Braida, W. and Ong, S.K. (2001). "Air sparging Effectiveness: Laboratory Characterization of Air-channel Mass Transfer Zone for VOC Volatilization." *Journal of Hazardous Materials*, B87: 241-258.

Johnson, R.L., Johnson, P.C., McWhorter, D.B., Hinchee, R.E., and Goodman, I. (1998). "An Overview of In situ Air Sparging." *Journal of Groundwater Monitoring and Remediation*, Vol. 13, Issue 4: 127-135.

Jones, T.B. (2003). "Basic Theory of Dielectrophoresis and Electrorotation," Journal *of IEEE Engineering in Medicine and Biology*, 0739-5175, Vol. 22, No. 6: 33.

Benner, M. L., Mohtar, R.H., and Lee, L.S. (2002). "Factors affecting air sparging remediation systems using field data and numerical simulations." *Journal of Hazardous Materials*, B95: 305–329

Cussler, E.L. (1997). *Diffusion, Mass Transfer in Fluid Systems*, Second Edition, Cambridge University Press, United Kingdom.

Suthersan, S.S. and Raton, B. (1999). "In-situ air sparging, Remediation engineering, design concepts." CRC Press LLC <Online at http://www2.bren.ucsb.edu/~keller/courses/esm223/SuthersanCh04AirSparge.pdf, last access January 2013>.

Vermeulen, F. and McGee, B., 2000, "In-situ electromagnetic heating for hydrocarbon recovery and environmental remediation," *Journal of Canadian Petroleum Technology*, Vol. 39, No. 8, pp. 25-29.